Sustainable Energy & Fuels

Efficient, Hysteresis Free, Inverted Planar Flexible Perovskite Solar Cells via Perovskite Engineering and Stability in Cylindrical Encapsulation

Journal:	*Sustainable Energy & Fuels*
Manuscript ID	SE-ART-03-2019-000153.R2
Article Type:	Paper
Date Submitted by the Author:	23-Apr-2019

Complete List of Authors:	Pandey, Manish; Kyushu Institute of Technology Kapil, Gaurav; University of Tokyo, Sakamoto, Kazuhiko; FUJICO CO. LTD. Hirotani, Daisuke; Kyushu Institute of Technology - Wakamatsu Campus, Kamarudin, Muhammad Akmal; Kyushu Institute of Technology - Wakamatsu Campus, Hamada, Kengo; Kyushu Institute of Technology Wang, Zhen; Kyushu Kogyo Daigaku - Wakamatsu Campus, Graduate School of Life Science and Systems Engineering Nomura, Daishiro; FUJICO CO. LTD. Kang, Hyo-Gyoung; FUJICO CO. LTD. Nagayoshi, Hideaki; FUJICO CO. LTD. Nakamura, Masaki; Ushio Inc., Hayashi, Masahiro; CKD Corporation Nomura, Takatoshi; CKD Corporation Hayase, Shuji; Kyushu Institute of Technology, Graduate School of Life Science and Systems Engineering

Efficient, Hysteresis Free, Inverted Planar Flexible Perovskite Solar Cells via Perovskite Engineering and Stability in Cylindrical Encapsulation

Manish Pandey[1,#,*], Gaurav Kapil[2], Kazuhiko Sakamoto[3], Daisuke Hirotani[1], Muhammad Akmal Kamrudin[1], Zhen Wang[1], Kengo Hamada[1], Daishiro Nomura[3], Hyo-Gyoung Kang[3], Hideaki Nagayoshi[3], Masaki Nakamura[4], Masahiro Hayashi[5], Takatoshi Nomura[5], Shuzi Hayase[1,*]

[1]Division of Green Electronics, Graduate School of LSSE, Kyushu Institute of Technology, 2-4 Hibikino, Wakamatsu, Kitakyushu, 8080196, Japan
Email: manish@life.kyutech.ac.jp, hayase@life.kyutech.ac.jp

[2]Research Center for Advanced Science and Technology, The University of Tokyo 4-6-1, Komaba, Tokyo,153-8904, Japan

[3]FUJICO CO. LTD., 4-31 Makiyamashinmachi, Tobata, kitakyushu, 804-0054, Japan

[4]Power System Department, Corporate R&D Division, USHIO.INC, 1194, Tosa, Besshomachi, Himeji, Hyogo, 671-0224 Japan

[5]CKD Corporation, 2-250, Ouji, Komaki, Aichi, 485-8551, Japan

Present Address: Laboratory for Organic Electronics, Division of Materials Science, Nara Institute of Science and Technology, 8916-5 Takayama-cho, Ikoma, Nara 630-0192, Japan

*Corresponding Author
manish.iitp12@gmail.com
hayase@life.kyutech.ac.jp

Abstract: A p-i-n type flexible perovskite solar cell (PSC) employing PEDOT:PSS as a hole transport material was fabricated implementing a synergistic approach to tune the composition and morphology of the perovskite films. This was accomplished by the optimization of methylammonium-formamidinium double-cation perovskite, $Pb(SCN)_2$ additive and different anti-solvents to make hysteresis-free flexible PSCs. PSCs being reported exhibit power conversion efficiency (PCE) of 16.13% with excellent mechanical stability, retaining > 90% of the PCE after 1000 bending cycles at the radius (R) of 6 mm. This PCE is amongst the highest reported values for the flexible inverted PSCs fabricated on PEDOT:PSS. Although PSCs on rigid conducting glass substrates have been reported to >20%, however, the long-term stability is of great concern because of poor encapsulation. Solution processibility of PSC gives the freedom to develop it on flexible substrate, which is suitable for

commercialization of PSCs. Herein, a novel encapsulation technology of sealing the flexible PSCs inside the cylindrical glass tubes (R = 8 mm) is being demonstrated. Encapsulated flexible devices retained 90% of PCE after 6000 hours under ambient conditions.

Keywords: flexible, perovskite engineering, encapsulation, cylindrical solar cells.

1. Introduction

Organolead triiodide perovskite-based solar cells (PSCs) have gained immense attention from the scientific community in the past few years due to the rapid increase in power conversion efficiency (PCE) from 3% to 23.3%.[1–8] More specifically, they are expected to be utilized as next-generation solar cells for portable and wearable electronics owing to their high power density and flexibility.[9,10] There are two kind of device structures widely used in PSCs, mesoporous or planar n-i-p structure utilizing n-type semiconductors such as (Titanium dioxide) TiO_2 and planar inverted p-i-n structure employing p-type semiconducting polymers such as poly(3,4-ethylenedioxythiophene):polystyrene sulfonate (PEDOT:PSS).[11] The mesoporous TiO_2 based PSCs are still leading in terms of efficiency due to their ability to form thick perovskite films for strong light absorption with high-quality of interfacial contacts by reducing interface recombination. These structures are well established in achieving PCE over 20%; however, they require high-temperature annealing at 450 °C which makes them not suitable for fabrication on flexible plastic substrates such as polyethylene terephthalate (PET) and polyethylene naphthalate (PEN).[11,12] As an alternative to these n-i-p type PSCs, inverted planar device architectures in p-i-n configuration involves the fabrication below 150 °C with the ability to demonstrate hysteresis-free high PCE.[7,11] Nevertheless, a lot of efforts are still going on in regular (n-i-p) and inverted (p-i-n) structures to reduce the processing temperature and hysteresis.[13]

In 2013, Docampo and coworkers have demonstrated the first flexible inverted PSC with a PCE of ~ 6% employing the inverted structure which involved the low-temperature solution processing of PEDOT:PSS as hole transporting material (HTM) and fullerene as electron transporting material (ETM). However, the PCE of PSCs utilizing the same HTM and ETM is not up to the mark till date.[9,10] Nowadays, the efficiency of flexible PSCs has reached >17% by employing several approaches such as demonstrating superior low-temperature processable charge extracting layers.[14–16] Despite the various advantages of flexible PSCs, inherent low transmittance and high resistance are hitches in the fabrication of high-quality charge transporting layers on flexible substrates. Besides, the low-temperature processing requirement further limits the deposition of thin films with superior quality, which affect the resultant PCE.[12,17–19] It is worth to note here that reported efficiencies for inverted flexible solar cells lag far behind, and apparently, the effort to optimize the PCE has been demonstrated for rigid glass substrates to a certain extent.

PSC is a heterojunction device where the quality of each interface is responsible for improved charge carrier extraction, however, morphology and composition of the perovskite layer is the most crucial one to affect the overall PCE. Therefore, optimizing the composition and morphology of the perovskite film have gained a lot of attention among the scientific community on rigid substrates and these things have not been yet fully utilized for flexible substrates, rather efforts have been made to exploit different electron and hole selective layers compatible for deposition on flexible substrates.[15,16] Mixing $MAPbI_3$ (methylammonium lead iodide) and $FAPbI_3$ (formamidinium lead iodide) is an effective approach to obtain the desired band gap for perovskite absorber films at a low temperature ~ 100 °C, popularly known as mixed cation perovskites. The $FAPbI_3$ possesses an ideal band gap (~ 1.4 eV) according to the Shockley- Queisser limit, however the film formation of pure $FAPbI_3$ needs annealing at ~ 150 °C due to the formation of a non-perovskite yellow (δ) phase at lower temperature.[20,21] It

has been demonstrated that a small fraction of MA^+ addition in $FAPbI_3$ would stabilize the perovskite phase and is now the well accepted recipe for the fabrication of high efficiency PSCs as well. The present work reports the similar strategy of fabrication on flexible substrates to achieve the higher efficiencies with step by step presentation of contribution by different components of flexible PSC.

PCE of PSCs is limited by the small grain size and low crystallinity as a result of a large number of radiative recombination arising from the high density of grain boundaries. However, there are various effective strategies exist where the grain size of the perovskite layers can be effectively increased by 200 nm to few micrometers by incorporating the additive lead thiocyanate ($Pb(SCN)_2$) in perovskite precursor. As a result of which, the density of the grain boundaries decreases, concomitantly increases the photogenerated carrier lifetime (τ) due to the passivation of grain boundaries by the formation of excess PbI_2.[22,23] At the same time, grain sizes relatively larger than the film thickness of the perovskite is sufficient for transporting the charge carriers at extracting interfaces, therefore the smoothness and absence of pin-hole in the perovskite films is of utmost requirement.[24] The control of such morphological features of the perovskite mostly relies on the deposition techniques as well as the conditions for perovskite films. 1-step method based coating is the simplest and most viable approach for in achieving high PCE, where the role of anti-solvent seems to be very critical as it speeds up the heterogeneous nucleation as discussed in detail previously.[25–29]

In this present work, keeping all the interfacial layers same for charge extractions in the device, the above effective strategies were synergistically utilized to improve the efficiency of the flexible PSCs. Therefore, all compositional and morphological engineering of the perovskite layer were carried out on the flexible substrates considering the possibility of any changes in the film formation arising from rheological behavior of the different solutions at different interfaces, and can vary from case to case. The different optimization

steps adopted, were as follows: 1) Optimization of perovskite composition using the MA and FA mixture, 2) optimization of the additives to tune the grain size of the perovskite and 3) the effect of different anti-solvents were explored taking the morphology into consideration and it was observed that all the 3-steps improved the overall efficiency of the flexible devices from ~ 10 % to 16.13 %. The efficiency achieved in this work is among the best-reported values of inverted flexible PSCs under similar device architectures using most conventional HTM (PEDOT:PSS) and ETM (C60). The observed changes in the perovskite films have been succefully characterized and correlated with the changes observed in electrical properties by utlizing different characterization techniques such as absorbance spectroscopy, X-Ray diffraction (XRD), Scanning electron microscopic (SEM) images, Atomic force microscopic (AFM) images, Photoluminescence (PL) and time resolved photoluminescence (TRPL) measurements.

Considering the stability of the flexible PSCs, albeit, significant improvement in PCE and efficient charge extracting materials for flexible substrates has been made in the recent years. Short lifetime of these devices and toxicity arising from hydrolysable lead-based perovskite is still a major hindrance in the commercialization of this technology so far. Recently, the lead-containing perovskite layer has been replaced by lead-free materials to produce PSCs. However, the poor stability of the highly efficient lead-based as well as lead-free PSCs has not yet been fully addressed.[30] Therefore, understanding the effect of encapsulation on the stability of the lead-based system would be helpful for future encapsulation of the lead-free system as well. Performance of these devices are extremely sensitive when operated or stored under ambient atmosphere; therefore, the preparation of flexible modules with adequately long operating lifetime needs to be addressed adequately. Moreover, long-term stability of these flexible devices also needs to be tested under the constant strain and performance should be ascertained as well and performance through bending cycles should not be tested alone

while considering real time applications in to account.[31] Although encapsulation of flexible PSCs has been demonstrated using plastic barrier materials to impede the ingress of moisture and oxygen for over 500 hours. These encapsulations strategies are rather incompetent considering the real-time applications where device needs to function in presence of strong wind and rain.[31] Therefore, in the present work, the flexible substrates were encapsulated in the cylindrical glass tubes of radius 8 mm under a nitrogen atmosphere (with H_2O and O_2 concentrations of < 0.1 ppm). The flexible devices were inserted in the bent-state to follow the curved surface of the tube to test not only the operational stability against atmospheric air but also when kept under constant strain. The stability test measurement of the cylindrically encapsulated flexible PSCs has showed very efficient stability retaining the 90% of its PCE under the long-term operation of 6000 h. To our knowledge, the present stability test result is longest durability test of any PSC, and the results obtained are among the best-reported values so far presented for flexible PSCs and is considerably higher even compared to the encapsulated rigid substrates.[31–33]

2. Results and Discussion

We fabricated the inverted PSC structure on flexible ITO/PET substrate with perovskite layer sandwiched between PEDOT: PSS as a HTM and C-60 as an ETM, and schematically shown together with their calculated energy levels in **Fig. 1**a,b. The absorption spectra of FA and MA mixed perovskites are shown in Fig. 1c, it is observed that the absorption is red shifted with an increase in FA concentration (0 to 30 %), which agrees to the previous reports,[34] leading to a higher photocurrent in comparison to monovalent cation-based perovskite absorber, $MAPbI_3$. Similarly, red-shift in the steady state photoluminescence spectra was also observed as shown in Fig. S1, which confirms the mixing of both the cations in perovskite crystals structure.[34] The XRD patterns of the films prepared by FA and MA mixture are shown in Fig. 1c. The diffraction peak (100) at $2\theta = 14.1°$ of $MAPbI_3$ continuously shifts to

lower angle with an increase in FA amount owing to the relatively larger ionic radius of FA in comparison to MA, which corresponds to increase in the size of the crystal lattice going to cubic or quasi-cubic phase,[35] It is worth mentioning that this gradual shift in the diffraction peak also confirms the presence of both FA and MA in the crystal lattice. As can be seen from the enlarge view of 110 peak that this peak is gradually shifting from 14.1° for X = 0 to 14.01° for X = 0.4. Moreover, the absence of any peaks related to pure $FAPbI_3$ and $MAPbI_3$ lattices confirms the absence of any phase segregation in the perovskite thin films.[34]

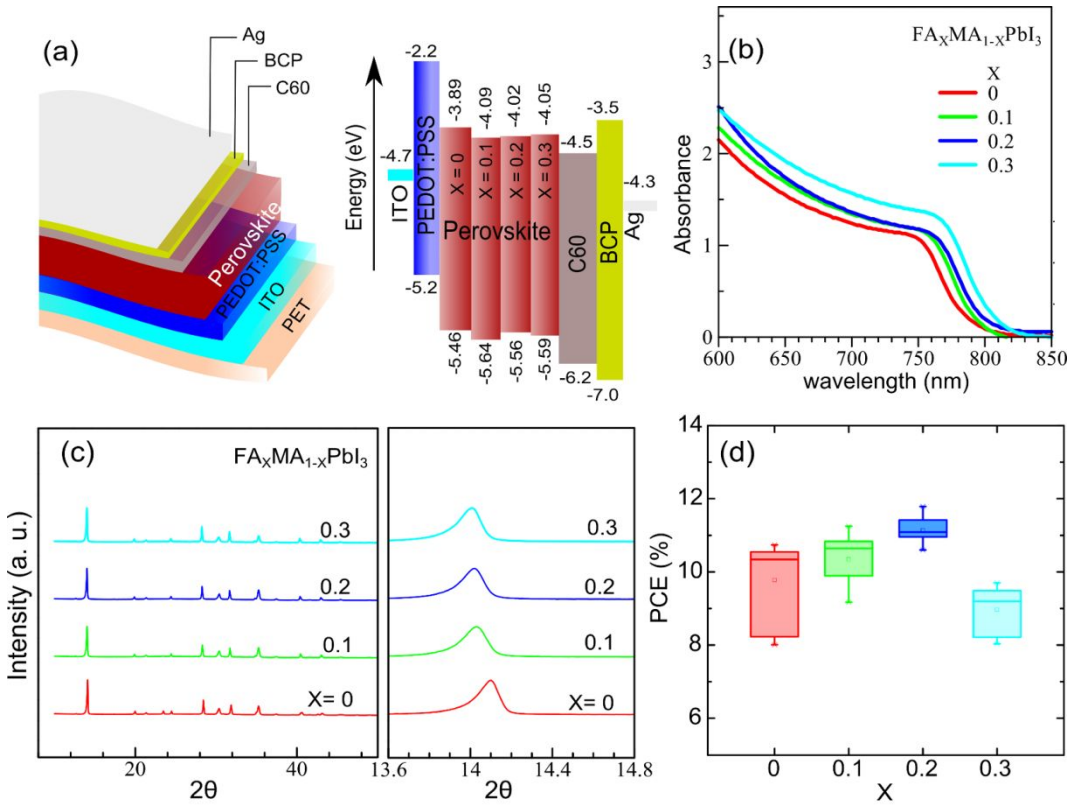

Fig. 1 (a) Fabrication sequence of each layer of perovskite with their energy levels. Absorbance (b) and XRD pattern (c) of $FA_XMA_{1-X}PbI_3$. (d) Box plot for PCE of flexible perovskite solar cells of $FA_XMA_{1-X}PbI_3$. The energy level of the perovskite layer shown in (a) HOMO energy and LUMO energy level of $FA_XMA_{1-X}PbI_3$ was estimated by absorption band edge and photoelectron yield spectroscopy (see in Fig. S2).

There are reports that for 1-step coating method,[26,27] where the use of toluene as an anti-solvent result in better perovskite film formation, therefore, to begin with, focus was given to the perovskite composition and toluene was used as the anti-solvent. Solar cells using FA and

MA mixtures were fabricated with X = 0 to X = 0.3 and optimized. The current voltage (J-V) characteristics were measured under 1-sun as shown in Fig. S1 with device parameters are given in the Table S1. The best PCE (11.13 %) was obtained with X = 0.2 (20% FA) in comparison to pure $MAPbI_3$ (9.78 %) as shown in the Fig. 1d. This enhancement of PCE is mainly attributed to the significant increase in the short-circuit current density (J_{SC}) and fill factor (FF) with FA and MA mixture, because of the increase in the red-shifted absorption (Fig. 1d). Similarly, red-shift was also observed in the corresponding incident photon to converted electron (IPCE) with FA addition as shown in Fig. S2. Full width at half maximum (FWHM) of the peak corresponding to (110) is increased with FA amount, which suggests in decrease of grain size and overall crystallinity of the FA rich films owing to the presence α-phase of $FAPbI_3$ which is thermally unstable and converts into δ-phase, hampering the single-phase crystallinity.[36] However, this increase in PCE resulted with 20% FA incorporation could be due increased τ as shown in Fig. S2 and red-shifted absorption as discussed above.[36] The solar cells with higher amount of FA (30%) addition shows decrease in photovoltaic performance because of increased radiative recombination, which could be assigned to the poor crystallinity and a shorter τ as shown in Fig. S2. Therefore, in result the best performance was obtained for $FA_{0.2}MA_{0.8}PbI_3$, which is selected to probe the effect of other factors.

It has been reported that the use of $Pb(SCN)_2$ additives in perovskite precursor tend to increase the grain size of the perovskite and improve the performance of PSCs. In our case, the concentration of this additive is varied from 3 to 6 wt% with respect to PbI_2 in the perovskite precursor solution in mixed cation perovskite composition, that is $FA_{0.2}MA_{0.8}PbI_3$.[22] The grain sizes of the perovskites were observed from the SEM images as shown in **Fig. 2**. The grain size ~ 100-250 nm of the perovskite film increases to ~ 1-2.5 μm with 3 wt% of $Pb(SCN)_2$, and further increases to ~ 3-5 μm with 6 wt% of $Pb(SCN)_2$. In comparison to the $FA_{0.2}MA_{0.8}PbI_3$ without $Pb(SCN)_2$, the intensity of the (110) diffraction

peak (2θ = 14.02°) of the perovskite shows a remarkable increase with $Pb(SCN)_2$, which indicate the high crystallinity of the films as shown in Fig. S3. It is also worth mentioning here that films fabricated with this additive led to the formation of excess PbI_2 as a bi-product due the mechanism involved in the formation of larger grain size as reported by Ke et al., the diffraction peak of PbI_2 was also observed at (2θ = 12.66°) reflecting the presence of it at grain boundaries or on the surfaces of the perovskite film, the PbI_2 presence can be seen in the SEM image (Fig. 2) as well.[22]

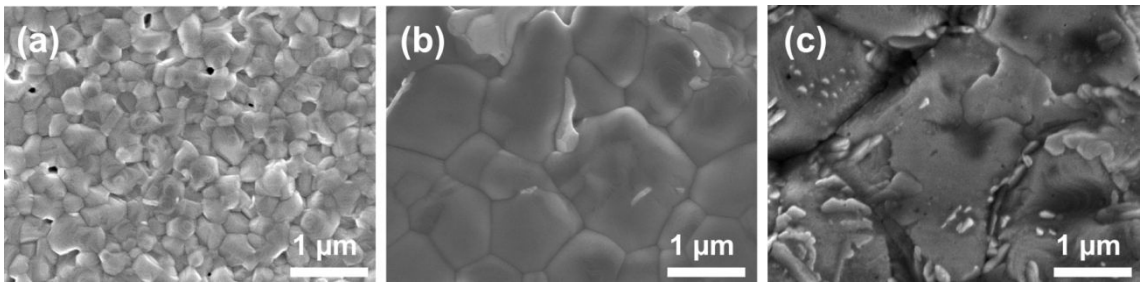

Fig. 2 Top view SEM images of perovskite films prepared on ITO/PET/PEDOT/PEDOT: PSS with varying amount of $Pb(SCN)_2$ additives. (a) 0 wt %, (b) 3 wt% and (c) 6 wt %.

The Dark and JV characteristics of the flexible PSCs based on $FA_{0.2}MA_{0.8}PbI_3$ with varying amount of $Pb(SCN)_2$ additives are shown in Fig. 3a, box chart of photovoltaic parameters are illustrated in Fig. S4 and Table S2. Consistent higher values of J_{SC} with an increase of open circuit voltage (V_{OC}) was observed in the devices with $Pb(SCN)_2$ in comparison to the devices without it, this results in increase of the overall PCE, which can be attributed to the enhancement in electrical properties of the perovskite film with enlarged grain size and less grain boundaries. As shown in Table S2, the optimized value of $Pb(SCN)_2$ concentration is found to be 3 wt% resulting in to the increase of average PCE of the flexible PSCs to 12.50 ± 0.38 % with J_{SC} = 19.02 ± 0.34 mA/cm^2, V_{OC} = 0.903 ± 0.009 V and FF = 0.721± 0.01 with a best PCE of 12.79%. The enhancement in Jsc with the incorporation of $Pb(SCN)_2$ was also confirmed by the higher IPCE (Fig. 3b). It is interesting to notice that a little broader IPCE spectrum was observed with the addtion of $Pb(SCN)_2$. Since $Pb(SCN)_2$ addition do not

changes absorption wavelength range as reported by others,[23,36] therefore, to further understand the mechanism for this enhancement, PL and TRPL measurements were conducted on the $FA_{0.2}MA_{0.8}PbI_3$ perovskite films with and without $Pb(SCN)_2$ as shown in the Fig. S5. In PL there was no significant difference in the peak wavelength, however, higher PL intensity in the films with additives was obtained which resulted in the increased τ and hence IPCE. The excited τ value for pure $FA_{0.2}MA_{0.8}PbI_3$ perovskite is 8.23 ns only, whereas the films prepared with 3 wt% $Pb(SCN)_2$ additives significantly improved the τ up to ~ 60-70 ns. Therefore, the large grain size of the perovskite reduces the photogenerated carrier recombination.[37] The decrease in overall PCE of the devices fabricated with a higher amount of $Pb(SCN)_2$ additives is attributed to the formation of an inhomogeneous film as well as due to the formation excess PbI_2 nanorods like structures at the interface which is agreement with the earlier reports.[22,23] The observed values of J_{SC} of the fabricated devices with and without $Pb(SCN)_2$ are also in good agreement with the integrated J_{SC} obtained by integrating the IPCE as shown in Fig. 3b.

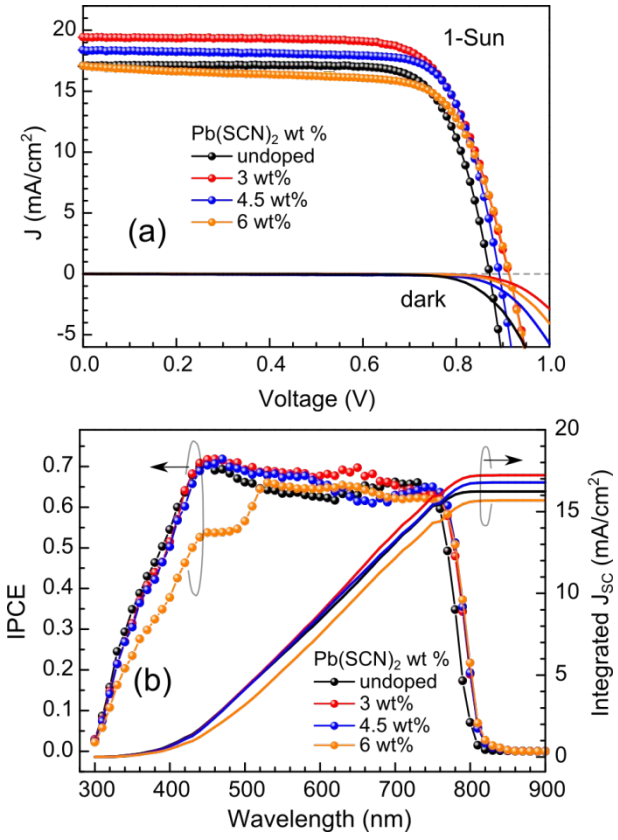

Fig. 3. JV characteristics of $Pb(SCN)_2$ doped devices under dark and 1-sun condition. (b) IPCE and integrated J_{SC} for $Pb(SCN)_2$ doped devices.

Choice of anti-solvent for dripping serves the crucial step to control the morphology of the perovskite films while film preparation through 1-step deposition method.[27] To probe the same, effect of different anti-solvents such as ethyl acetate (ETAC), Chlorobenzene (CB) and Toluene (TOL) were examined on optimized mixed cation composition with $Pb(SCN)_2$. Irrespective of the grain sizes produced by dripping different anti-solvents, the distribution and uniformity of films produced also play a major role in solar cell activity. The different antisolvents employed in the study have major effect on the grain sizes and surface roughness of the films as observed by SEM and AFM images shown in Fig. S6, however, thickness of films does not change with anti-solvents and lies around ~ 450 – 475 nm. The SEM and AFM images revealed that ETAC based films possesses highest surface uniformity. On the other hand, the grain size followed the trend TOL > CB > ETAC. To examine the difference further, PL and TRPL measurements were carried for all the films as shown in Fig. 4. The increased PL intensity with decrease in FWHM (41.95°) for the case of films prepared by ETAC followed by TOL (42.27°) and CB (42.73°) indicates for better LUMO to HOMO transition with less trap energy levels resulting into decreased non-radiative recombination, which is the signature of better performing absorber layer for solar cells.[38] Interestingly, a blue shift was noticed with the films prepared by TOL, when compared to films fabricated using CB. The PL peak is further blue shifted with ETAC employed films, which is an indication of reduced thermal losses or existence of less energy levels between conduction band minimum (CBM) and valence band maximum (VBM) in comparison to TOL and CB based films. The observed value for τ was 124.1 ns for ETAC dripped films in comparison to 60.5 ns for Toluene and 40.5 ns in CB dripped films. The increase of τ in the case of ETAC based films, clearly

suggest for uniform, pin-hole free films with well distributed grain sizes, which is an important criterion for better solar cell performance.

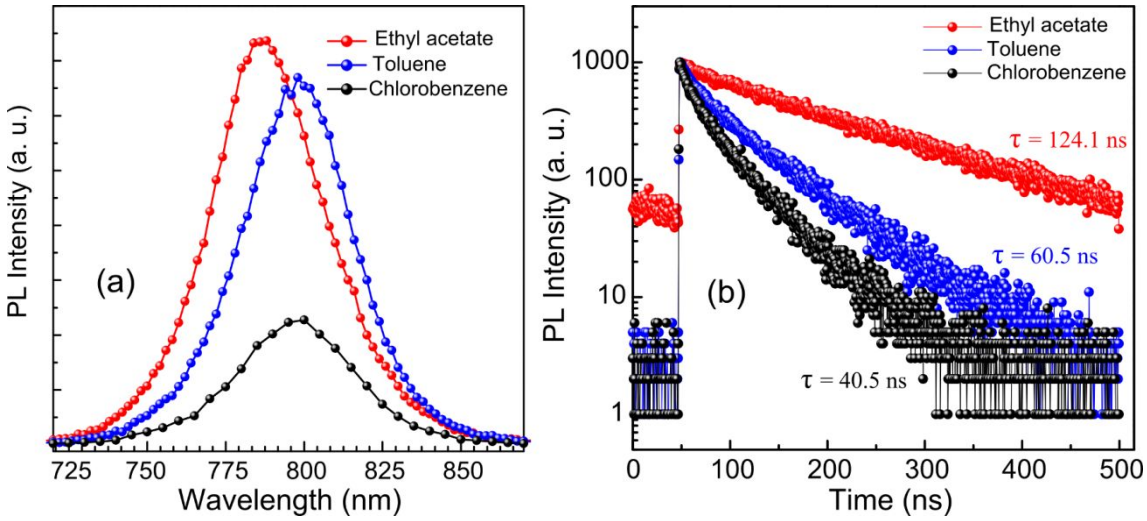

Fig. 4. Photoluminescence response of $FA_{0.2}MA_{0.8}PbI_3$ (having $Pb(SCN)_2$ additives) perovskite films prepared on glass substrates by dripping different anti-solvents. (a) steady-state PL and (b) time-resolved PL decay transients.

It has already been reported that the anti-solvent has major effect on the photovoltaic characteristics due to the perovskite film's morphology change as reported earlier by other.[27,39] Therefore, to evaluate the effect of morphology change on solar cell performance the Dark and JV characteristics of the flexible PSCs were obtained as shown in **Fig. 5**a with photovoltaic parameter details in **Table 1**. The perovskite thin films prepared with ETAC as anti-solvents yielded an average J_{SC} of 21.02 mA/cm^2, V_{OC} of 0.92 V and FF of 0.78. The average PCE of the devices containing perovskite layer dripped with ETAC was significantly high at 15.04 ± 0.46 % and reaches up to 16.13% in comparison to that of 12.44 ± 0.30 % (12.84) for TOL and 10.12 ± 0.85 % CB (10.96) dripped perovskite-based flexible PSCs. The IPCE spectra and integrated J_{SC} of the flexible PSCs prepared with different anti-solvents are shown in Fig. 5b, where integrated J_{SC} obtained is in good agreement with the obtained J_{SC}

from IV measurement of the devices. The IPCE values for devices prepared with ETAC exceeded 80% in the range of 420 to 780 nm and reaches up to a maximum 85% around 720 nm. The IPCE has uniformly increased in the entire wavelength region in comparison to TOL and CB based solar cells. This increase can be either due to the difference in film thickness or is the effect of different rate of charge recombination leading to different open circuit voltage (V_{OC}) and hence, J_{SC}. As it was mentioned earlier that film thickness was negligibly affected by the anti-solvent used, therefore, the uniform IPCE increment can be answered by the reduction in voltage loss with ETAC employed films. This reduced recombination loss or voltage loss in case of ETAC dripped films is well reflected in least series resistance (4.26 ± 0.35 Ω) and improved fill factor (0.78 ± 0.015).

Table 1. Photovoltaic parameters of the $FA_{0.2}MA_{0.8}PbI_3$ having 3 wt% of $Pb(SCN)_2$ prepared with different anti-solvents under forward scan. Box plot of each parameter of the devices is given in the Fig. S7 and Fig. S8.

Anti-solvent	J_{SC} (mA/cm^2)[a)]	V_{OC} (V)[a)]	FF[a)]	R_S (Ω)[b)]	PCE (%)[a)]
Ethyl acetate	21.02 ± 0.52 (21.76)	0.92 ± 0.025 (0.968)	0.78 ± 0.015 (0.799)	4.26 ± 0.35 (3.63)	15.04 ± 0.46 (16.13)
Toluene	19.03 ± 0.39 (19.70)	0.90 ± 0.009 (0.918)	0.72 ± 0.015 (0.736)	6.09 ± 0.95 (5.18)	12.44 ± 0.30 (12.84)
Chlorobenzene	16.16 ± 1.34 (17.68)	0.85 ± 0.008 (0.862)	0.74 ± 0.02 (0.775)	5.67 ± 1.03 (4.62)	10.12 ± 0.85 (10.96)

[a)]Values in brackets represent maximum. [b)]Values in the bracket represent minimum.

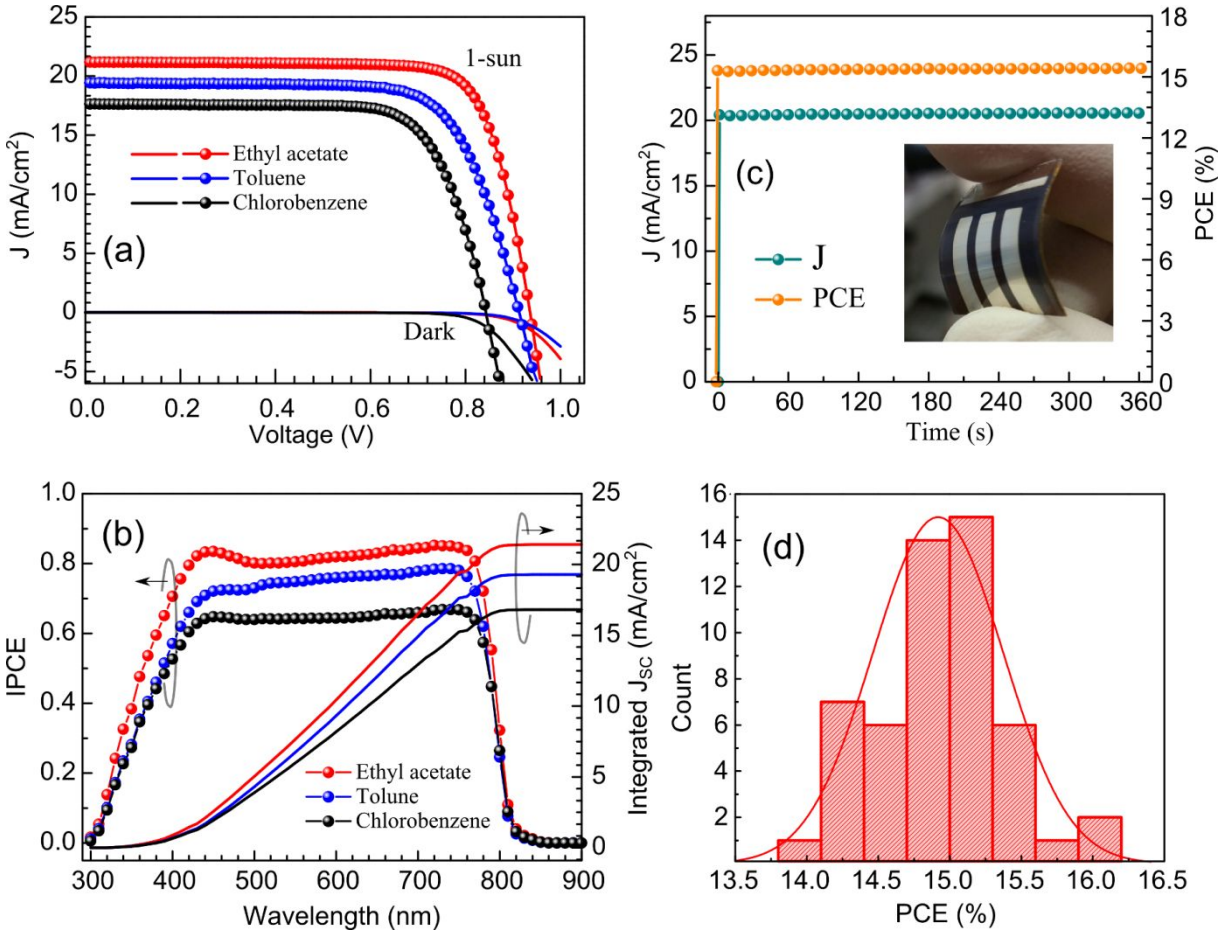

Fig. 5. JV characteristics (a), IPCE and integrated current density of flexible PSCs prepared with $FA_{0.2}MA_{0.8}PbI_3$ having 3 wt% $Pb(SCN)_2$ additive using different anti-solvents. Maximum power point tracking at 0.75 V (c) and histogram (d) of the flexible PSCs prepared with Ethyl acetate anti-solvent.

It has been reported that inverted (p-i-n) device structures exhibit low hysteresis in the forward and reverse scan.[11,40] To precisely examine the PCE of the flexible device, we measured the steady-state current density at a forward bias of 0.75 V (corresponds to maximum power point) as shown in Fig. 5c and device yielded a stabilized current density of 20.5 mA/cm^2, output PCE of 15.42%. To our knowledge, this PCE is among the highest PCE observed in inverted flexible PSCs with conventional PEDOT:PSS and C60 charge extracting layers and is comparable to best reported values using various ETL and HTM as well (see Table S3).[9,10] The prepared devices were almost hysteresis free as shown in Fig. S9 and Fig. S10. As performance reproducibility is of high concern for researchers, reproducibility of the

devices was tested by fabricating more than 50 devices in 4 different batches as shown in Fig. 5d, indicating high reproducibility of the flexible device.

Harsh bending conditions are of great concern for practical applications of flexible PSCs to qualify for portable and wearable electronics applications. To examine this, mechanical flexibility and durability of the flexible PSCs were carried out. Same flexible PSC was bent once across the cylindrical tubes of different radii (r = 10, 8, 6, 4 and 2 mm) as shown in **Fig. 6**a. The PCE of the device showed no decrease up to 4 mm and retained 92% of initial PCE at 2 mm in comparison to the performance at without bending condition. Zardetto et al. have extensively examined the conductivity of the ITO electrode on a different flexible substrate and found substantially increased sheet resistance for bending radii of < 4 mm due to crack formation on ITO films because of its brittle nature. Therefore, this retardation of PCE is due to decrease in the conductance of the ITO layer which takes place when bent at raddi < 4 mm.[12] As a consequence, the bending of PET/ITO/Perovskite results in crack formation as already reported.[41] Therefore, the decrease in PCE when bent at radii of < 4 mm is attributed to crack formation of ITO electrodes which is also confirmed for our case as shown in Fig. S11.

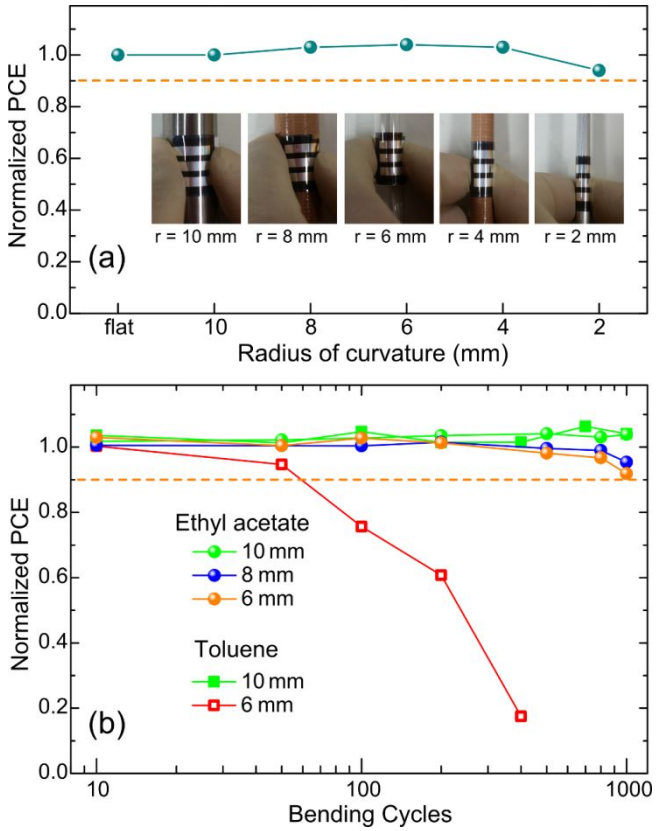

Fig. 6. (a) Normalized PCE of the devices prepared with bent ethyl acetate as antisolvents at bent at different radius with respect to flat (r = 0 mm). The photograph taken while bending flexible PSCs at different radii (r = 10, 8 and 6 mm) is shown in the inset. (b) Normalized PCE with bending cycles for the devices prepared by Ethyl acetate and toluene at different radius of curvatures.

To further examine the effect of bending, flexible PSCs were tested via multiple-cycle bending at different radii (r = 10, 8 and 6 mm). Bending up to 1000 cycles were performed on devices prepared by different anti-solvent (ETAC and toluene) as shown in Fig. 6b. Devices prepared with ETAC showed excellent bending test maintaining > 90% efficiency of the initial value up to 1000 bending at different radii (10, 8, and 6 mm). On the other hand, PCE of the devices prepared with toluene decreases substantially < 20% of the original value at 400 bending cycles at r = 6 mm. These superior bending results in the present case must be attributed to quality of the perovskite film since the thickness of other ETM, HTM layers and PET/ITO substrates were same. Therefore, this high quality bending test in the flexible PSCs

can be ascribed to the high quality perovskite films prepared with ETAC as anti-solvent and role of anti-solvent is very important to prepare compact hole free perovskite films to exhibit high mechanical flexibility as discussed above.[24] Bending PET/ITO/Perovskite up to 1000 cycles retained > 90% of the efficiency (comparison table of the recent reports can be seen in Table S4.

Our research group has previously shown the advantages associated with the cylindrical type solar cells where it can harvest the light from all other directions and are beneficial for numer of applications.[42] The main aim of the stability test was to investigate the durability of cylindrical encapsulated flexible PSCs (will be called as encapsulated from now) is shown in **Fig. 7**. It is worth mentioning, that the flexible PSCs with dimension (2 × 2 cm) were inserted and placed carefully in the cylindrical tube to follow its curvature (r = 8 mm) so that the device stability can be observed under the strain as well. To make a relative comparison, both kinds of devices (encapsulated and non-capsulated) were also left under in ambient laboratory atmosphere, at temperature range of 22-30 °C and relative humidity of 40 to 80%. The JV characteristics of both were periodically measured at different intervals up to 6000 h, till the preparation of this report. The JV parameters for the encapsulated and non-encapsulated device recorded are shown in **Fig. 7**. Performance of the devices without encapsulation started degrading within 24 hours and degraded up to 25% of its initial value in 133 h, < 50% of initial value in 342 h and reaches to 0 in ~ 1000 h. On the other hand, encapsulated devices retained almost 100% of the initial values up to ~4200 h and PCE retained 90% of its initial value up to 6000 h (Fig. 7a). This performance retained over a period of 6000 h is the highest durability measured for pure 3-D perovskite based solar cells.[32,33,43] Recently, use of 2D/3D mixed perovskite layers seems to be promising in improving the stability,[44,45] and Nazeeruddin and coworkers have demonstrated that when 2D/3D perovskite used in combination with carbon based electrode, stability of over 1 year

can be easity achived.[44] Therefore, the devices stability even in the bent state suggest the promising future of the flexible PSCs for wearable electronics.

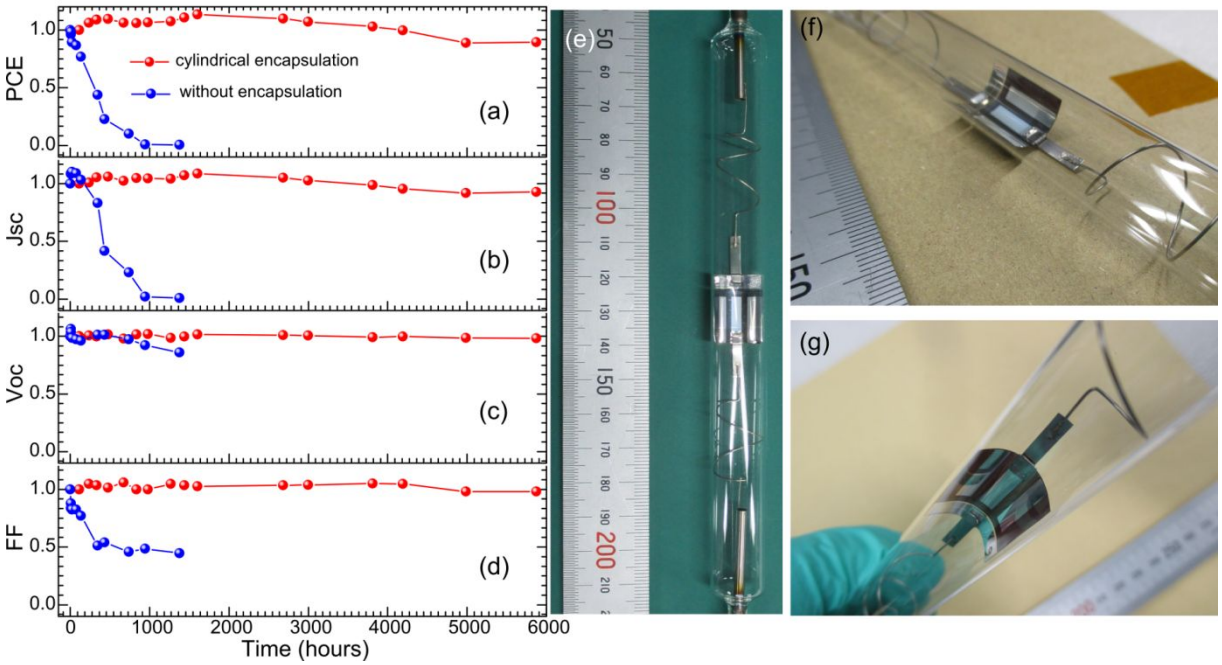

Fig. 7. Long-term stability test of the flexible PSCs left in encapsulated in cylindrical type and without encapsulation (a-d). Photograph of the cylindrical type encapsulated device from different angle (e-g).

Flexible PSCs are indeed the promising candidates for roll-to-roll production to be utilize in wearable and printable power sources. However, the present cylindrical encapsulation is intentionally done for futuristic power sources to utilize the flexible cells in shapes similar to fluorescent lamps where they will be capable of harvesting light from all the directions with high resistance towards strong wind and snow. Apart from this, the installation of such cells would occupy small space and the output power could be utilized for farming land, remote sensing machines. Moreover, to realize such devices outside, long-term stability test under high temperature and humid conditions with the mechanism involved is under study and will be reported separately.

3. Conclusion

Compositional engineering of double-cation ($FA_XMA_{1-X}PbI_3$) perovskite and use of $Pb(SCN)_2$ additives in perovskite precursor solution is demonstrated in the inverted flexible PSCs. It was explored that a mixture of FA and MA cation-based PSCs exhibited an increased absorption edge towards longer wavelength increasing the overall current density in comparison to only MA based PSCs leading to a maximum PCE of 11.13 ± 0.36 %. Further increase in solar cell performance to 12.50408 ± 0.38 % was resulted with the use of $Pb(SCN)_2$ additive in the optimized $FA_{0.2}MA_{0.8}PbI_3$ perovskite layer, due to significant increase in the grain size, concomitantly prolonged τ. Moreover, in the optimized perovskite composition with the additive, the effect of different antisolvents such as ethyl acetate, toluene and chlorobenzene were also examined. The films prepared with ethyl acetate displayed a pin-hole free, dense and smooth surface enabling to a better interfacial contact with ETM (C_{60}) layer, which further led to the hysteresis free PCE of 15.04 ± 0.46 % with maximum up to 16.13%, best reported value for flexible solar cells prepared on PEDOT:PSS. The bending test of the flexible devices revealed that the uniform film exhibited high durability against bending, retaining > 90% of the original PCE. The stability of the encapsulated device in form of cylindrical tube revealed that the device retained ~ 90%, suggesting no ingress of humidity and oxygen through it. These results clearly reflect that the flexible PSCs cells can be rolled in different shapes and can be made printing compatible that would be capable of producing high output power and in different kind of shapes towards futuristic power sources.

4. Experimental Section

4.1. Materials and methods: PET-ITO substrates with resistance 60 Ω/□ were purchased from Sigma Aldrich. PET-ITO substrates were etched from one side with the mixture of zinc powder (Wako, JAPAN) and diluted HCl (Wako, JAPAN) followed by the removal of the residual dried zinc powder with water using cotton bud. All substrates were sequentially

washed in a soap solution, ethanol (Wako, Japan) and distilled water, followed by drying in a vacuum oven at 60° C overnight. PEDOT:PSS (Clevios™ PVP AI 4083) was used as received, is filtered with PVDF filters (pore size 0.45 μm) before coating on the substrates. All the solvents to prepare perovskite precursor solution and anti-solvents for dripping were anhydrous, purchased from Sigma Aldrich (USA).

4.2. Device Fabrication: The flexible substrates were mounted on rigid glass substrates from edges which can facilitate the easy spin coating and make them flat to get uniform films. An oxygen plasma treatment of 15 mins on cleaned substrates was done, prior to coat PEDOT:PSS (Clevious Clevios™ PEDOT:PSS PVP AI 4083). The PEDOT:PSS was spin coated at 4000 r.p.m. for 50 secs followed by annealing on hot plate at 145 °C for 30 minutes. The films were then transferred to glovebox equipped with constant nitrogen flow (O_2 < 0.1 ppm and H_2O < 0.1 ppm), for the perovskite layer coating. 1.3 M precursor solution was prepared by mixing various ratio of FAI, MAI, and PbI_2 (all from Tokyo Chemical Industry, Japan) in the mixture of N,N-dimethylformamide/ dimethyl sulfoxide (4:1). For $Pb(SCN)_2$ additive containing precursor solutions, $Pb(SCN)_2$ was added separately to the perovskite precursor solutions in the required amount and the weight ratio was kept 3, 4.5 and 6 wt% with respect to weight of PbI_2. The solutions were stirred for 1 h at room temperature. A 100 μl of perovskite solution was dropped and spun at 1000 rpm for 10s followed by 4000 rpm for 30 s, a 600 μl of antisolvent was dripped at the 5^{th} s during second spin rate. The substrates were annealed on a hot plate at 105°C for 10 minutes. On the top of perovskite film Fullerene (C60) (nanom purple SC) (25 nm), bathocuproine (BCP) (Sigma-Aldrich, 99%) (5 nm) and silver electrodes (Ag) (120 nm) were sequentially deposited by thermal evaporation (10^{-4} Pa).

4.3. Film and Device Characterization: XRD measurements were performed in the out-of-plane mode with Rigaku smart lab X-ray diffractometer with Cu Kα radiation (1.5418 angstrom) operated at 45 KV (200 mA). Absorbance spectra were recorded with Shimadzu

UV-2550 spectrophotometer. SEM images were taken with JEOL EOS (6701). PL and TRPL measurements were performed in ambient air with Hamamatsu fluorescence lifetime spectrometer C11367 equipped with Hamamatsu picosecond light pulser (C10196). Perovskite samples were illuminated from the film side with a continuous laser beam having 465 nm wavelength. Thickness of each thin films were measured by interference microscopy (Nikon Eclipse LV-150). AFM images were taken using a JEOL SPM 5200 having Olympus (OMCL-AC200TS-C3) probes operated under tapping mode to investigate the surface morphology. The JV characteristics of flexible devices were measured in ambient atmosphere with solar simulator (KHP-1, Bunko-Keiki) under AM 1.5 illumination adjusted to the output intensity of 100 mW/cm^2 using spectroradiometer, which was also confirmed by reference silicon solar cell (BS-520 S/N 007, Bunko-Keiki, Japan). IPCE spectra were recorded by the same instrument under short circuit conditions. The device area exposed to light was 10 mm^2 using a black metal mask, however, in case of the cylindrically encapsulated device the area for the respective device was calculated with an optical microscope and used without any mask. Bending test measurement was performed by bending the solar cells across the cylindrical rods having different radii (10, 8, 6, 4 mm) with electrodes along the curvature of the rod.

4.4. Cylindrical Encapsulation and stability measurement: The connections to flexible solar cells were first made with the titanium wire, and titanium wire were bend in spiral shape away from the device to so that the flexible substrates can bend and follow the peripheral of the cylindrical tube (radius 8mm) as shown in Fig. 7e. Later, under nitrogen atmosphere having oxygen and H_2O values < 0.1 ppm, the cylindrical glass tubes were sealed using the flame with titanium terminals left out at the edge for connections.

Corresponding Author

*Manish Pandey (manish.iitp12@gmail.com)
ORCID : 0000-0003-0963-8097

*Shuzi Hayase (hayase@life.kyutech.ac.jp)

Notes
Authors declare no competing financial interests.

Acknowledgement

This research was financially supported by S-Innovation.

Statement of Contribution

MP, GK, KS and SH conceived the idea and designed all the experiments. MP fabricated all the devices and the samples for characterizations. MP, DH, KH and MAK conducted the photoluminescence and absorbance measurement. MP and MAK conducted the XRD measurement. MP and ZW performed the SEM measurement. DN, HGK and HN fabricated and optimized the cylindrical glass tube. MN, MH, KS and TN encapsulated the device and performed the electrical measurement. MP and GK analyzed all the results and wrote the manuscript. SH supervised the project.

References

1 A. Kojima, K. Teshima, Y. Shirai and T. Miyasaka, *J. Am. Chem. Soc.*, 2009, **131**, 6050–6051.

2 H. S. Kim, C. R. Lee, J. H. Im, K. B. Lee, T. Moehl, A. Marchioro, S. J. Moon, R. Humphry-Baker, J. H. Yum, J. E. Moser, M. Grätzel and N. G. Park, *Sci. Rep.*, 2012, **2**, 591.

3 W. S. Yang, B.-W. Park, E. H. Jung, N. J. Jeon, Y. C. Kim, D. U. Lee, S. S. Shin, J. Seo, E. K. Kim, J. H. Noh and S. Il Seok, *Science*, 2017, **356**, 1376–1379.

4 M. M. Lee, J. Teuscher, T. Miyasaka, T. N. Murakami and H. J. Snaith, *Science*, 2012, **338**, 643–7.

5 H. J. Snaith, *J. Phys. Chem. Lett.*, 2013, **4**, 3623–3630.

6 M. A. Green, A. Ho-Baillie and H. J. Snaith, *Nat. Photonics*, 2014, **8**, 506–514.

7 D. Luo, W. Yang, Z. Wang, A. Sadhanala, Q. Hu, R. Su, R. Shivanna, G. F. Trindade, J. F. Watts, Z. Xu, T. Liu, K. Chen, F. Ye, P. Wu, L. Zhao, J. Wu, Y. Tu, Y. Zhang, X.

Yang, W. Zhang, R. H. Friend, Q. Gong, H. J. Snaith and R. Zhu, *Science*, 2018, **360**, 1442–1446.

8 NREL, Best Research-Cell Efficiencies., https://www.nrel.gov/pv/assets/pdfs/pv-efficiency-chart.201812171.pdf, (accessed 18 December 2018).

9 B. Susrutha, L. Giribabu and S. P. Singh, *Chem. Commun.*, 2015, **51**, 14696–14707.

10 L. Li, S. Zhang, Z. Yang, E. E. S. Berthold and W. Chen, *J. Energy Chem.*, 2018, **27**, 673–689.

11 L. Meng, J. You, T.-F. Guo and Y. Yang, *Acc. Chem. Res.*, 2016, **49**, 155–165.

12 V. Zardetto, T. M. Brown, A. Reale and A. Di Carlo, *J. Polym. Sci. Part B Polym. Phys.*, 2011, **49**, 638–648.

13 S. A. L. Weber, I. M. Hermes, S.-H. Turren-Cruz, C. Gort, V. W. Bergmann, L. Gilson, A. Hagfeldt, M. Graetzel, W. Tress and R. Berger, *Energy Environ. Sci.*, 2018, **11**, 2404–2413.

14 F. Yang, J. Liu, H. E. Lim, Y. Ishikura, K. Shinokita, Y. Miyauchi, A. Wakamiya, Y. Murata and K. Matsuda, *J. Phys. Chem. C*, 2018, **122**, 17088–17095.

15 W. Chen, Y. Wu, J. Fan, A. B. Djurišić, F. Liu, H. W. Tam, A. Ng, C. Surya, W. K. Chan, D. Wang and Z.-B. He, *Adv. Energy Mater.*, 2018, **8**, 1703519.

16 H. Dong, Z. Wu, J. Xi, X. Xu, L. Zuo, T. Lei, X. Zhao, L. Zhang, X. Hou and A. K.-Y. Jen, *Adv. Funct. Mater.*, 2018, **28**, 1704836.

17 L. Hao, X. Diao, H. Xu, B. Gu and T. Wang, *Appl. Surf. Sci.*, 2008, **254**, 3504–3508.

18 K.-S. Tseng and Y.-L. Lo, *Opt. Mater. Express*, 2014, **4**, 764.

19 C. Wang, L. Guan, D. Zhao, Y. Yu, C. R. Grice, Z. Song, R. A. Awni, J. Chen, J. Wang, X. Zhao and Y. Yan, *ACS Energy Lett.*, 2017, **2**, 2118–2124.

20 G. E. Eperon, S. D. Stranks, C. Menelaou, M. B. Johnston, L. M. Herz and H. J. Snaith, *Energy Environ. Sci.*, 2014, **7**, 982.

21 S. Pang, H. Hu, J. Zhang, S. Lv, Y. Yu, F. Wei, T. Qin, H. Xu, Z. Liu and G. Cui, *Chem. Mater.*, 2014, **26**, 1485–1491.

22 W. Ke, C. Xiao, C. Wang, B. Saparov, H.-S. Duan, D. Zhao, Z. Xiao, P. Schulz, S. P. Harvey, W. Liao, W. Meng, Y. Yu, A. J. Cimaroli, C.-S. Jiang, K. Zhu, M. Al-Jassim, G. Fang, D. B. Mitzi and Y. Yan, *Adv. Mater.*, 2016, **28**, 5214–5221.

23 Y. Yu, C. Wang, C. R. Grice, N. Shrestha, J. Chen, D. Zhao, W. Liao, A. J. Cimaroli, P. J. Roland, R. J. Ellingson and Y. Yan, *ChemSusChem*, 2016, **9**, 3288–3297.

24 T. Ye, S.-L. Lim, X. Li, M. Petrović, X. Wang, C. Jiang, W.-P. Goh, C. Vijila and S. Ramakrishna, *Sol. Energy Mater. Sol. Cells*, 2018, **175**, 111–117.

25 Y. Zhou, O. S. Game, S. Pang and N. P. Padture, *J. Phys. Chem. Lett.*, 2015, **6**, 4827–4839.

26 K.-M. Lee, C.-J. Lin, B.-Y. Liou, S.-M. Yu, C.-C. Hsu, V. Suryanarayanan and M.-C. Wu, *Sol. Energy Mater. Sol. Cells*, 2017, **172**, 368–375.

27 S. Paek, P. Schouwink, E. N. Athanasopoulou, K. T. Cho, G. Grancini, Y. Lee, Y. Zhang, F. Stellacci, M. K. Nazeeruddin and P. Gao, *Chem. Mater.*, 2017, **29**, 3490–3498.

28 Z. Huang, D. Wang, S. Wang and T. Zhang, *Materials (Basel).*, 2018, **11**, 778.

29 J. Troughton, K. Hooper and T. M. Watson, *Nano Energy*, 2017, **39**, 60–68.

30 Z. Shi, J. Guo, Y. Chen, Q. Li, Y. Pan, H. Zhang, Y. Xia and W. Huang, *Adv. Mater.*, 2017, **29**, 1605005.

31 H. C. Weerasinghe, Y. Dkhissi, A. D. Scully, R. A. Caruso and Y.-B. Cheng, *Nano Energy*, 2015, **18**, 118–125.

32 A. Mei, X. Li, L. Liu, Z. Ku, T. Liu, Y. Rong, M. Xu, M. Hu, J. Chen, Y. Yang, M. Grätzel and H. Han, *Science*, 2014, **345**, 295–8.

33 F. Bella, G. Griffini, J.-P. Correa-Baena, G. Saracco, M. Grätzel, A. Hagfeldt, S. Turri and C. Gerbaldi, *Science*, 2016, **354**, 203–206.

34 Y. Zhang, G. Grancini, Y. Feng, A. M. Asiri and M. K. Nazeeruddin, *ACS Energy Lett.*, , DOI:10.1021/acsenergylett.7b00112.

35 N. J. Jeon, J. H. Noh, W. S. Yang, Y. C. Kim, S. Ryu, J. Seo and S. Il Seok, *Nature*, 2015, **517**, 476–480.

36 C. Wang, D. Zhao, Y. Yu, N. Shrestha, C. R. Grice, W. Liao, A. J. Cimaroli, J. Chen, R. J. Ellingson, X. Zhao and Y. Yan, *Nano Energy*, 2017, **35**, 223–232.

37 Y. Wu, F. Xie, H. Chen, X. Yang, H. Su, M. Cai, Z. Zhou, T. Noda and L. Han, *Adv. Mater.*, 2017, **29**, 1701073.

38 H. Huang, M. I. Bodnarchuk, S. V. Kershaw, M. V. Kovalenko and A. L. Rogach, *ACS Energy Lett.*, 2017, **2**, 2071–2083.

39 J. Ha, H. Kim, H. Lee, K.-G. Lim, T.-W. Lee and S. Yoo, *Sol. Energy Mater. Sol. Cells*, 2017, **161**, 338–346.

40 Y. Li, L. Meng, Y. (Michael) Yang, G. Xu, Z. Hong, Q. Chen, J. You, G. Li, Y. Yang and Y. Li, *Nat. Commun.*, 2016, **7**, 10214.

41 J. Feng, X. Zhu, Z. Yang, X. Zhang, J. Niu, Z. Wang, S. Zuo, S. Priya, S. F. Liu and D. Yang, *Adv. Mater.*, 2018, **30**, 1801418.

42 J. Usagawa, S. S. Pandey, Y. Ogomi, S. Noguchi, Y. Yamaguchi and S. Hayase, *Prog.*

Photovoltaics Res. Appl., 2013, **21**, 517–524.

43 Y. Il Lee, N. J. Jeon, B. J. Kim, H. Shim, T.-Y. Yang, S. Il Seok, J. Seo and S. G. Im, *Adv. Energy Mater.*, 2018, **8**, 1701928.

44 G. Grancini, C. Roldán-Carmona, I. Zimmermann, E. Mosconi, X. Lee, D. Martineau, S. Narbey, F. Oswald, F. De Angelis, M. Graetzel and M. K. Nazeeruddin, *Nat. Commun.*, 2017, **8**, 15684.

45 F. Yang, P. Zhang, M. A. Kamarudin, G. Kapil, T. Ma and S. Hayase, *Adv. Funct. Mater.*, 2018, **28**, 1804856.

Table of Content:

Efficient flexible perovskite solar cells by compositional engineering. Cylindrically encapsulated devices retained 90% of the device efficiency after 6000 h.